

Sea surface paleoproductivity reconstruction based on foraminiferal accumulation rate in the western Savu Strait since the Last Glacial Maximum (~23 ka BP)

Rudarsko-geološko-naftni zbornik
(The Mining-Geology-Petroleum Engineering Bulletin)
UDC: 56:579; 550.8; 551.58; 551.8
DOI: 10.17794/rgn.2023.1.14

Original scientific paper



Ryan Dwi Wahyu Ardi^{1,2}; Aswan¹; Khoiril Anwar Maryunani¹; Eko Yulianto³; Purna Sulastya Putra^{1,3}; Septriono Hari Nugroho^{1,3}

¹ Geological Engineering Study Program, Faculty of Earth Science and Technology, Institut Teknologi Bandung, Jl. Ganesha No. 10 Bandung 40132, <https://orcid.org/0000-0002-2037-9287> (RDWA)

² Agrotechnology Study Program, Faculty of Science and Technology, Universitas Nahdlatul Ulama Purwokerto, Jl. Sultan Agung No. 42 Purwokerto 53144

³ Research Centre for Geological Disaster, National Research and Innovation Agency, Jl. Sangkuriang Bandung 40135, <https://orcid.org/0000-0002-4417-5852> (PSP), <https://orcid.org/0000-0001-5501-3608> (SHN)

Abstract

Despite its importance, sea surface paleoproductivity of the western Savu Strait is not well studied. Results from previous study at the nearby Southwest Sumba and Sumba Strait might not be applicable due to the oceanographic difference. Foraminiferal proxies from gravity core ST10 were applied to generate sea surface paleoproductivity and thermocline depth reconstruction. Foraminiferal Accumulation Rate and Benthic Foraminiferal Accumulation Rate were used as paleoproductivity proxies while the thermocline dwellers' relative abundance was applied as the thermocline depth proxy. This study suggested paleoproductivity increase during the Last Glacial Maximum (LGM)~16 ka BP and Holocene (after ~11.65 ka BP) in the western Savu Strait. Thermocline depth was relatively shallower during the LGM–Last Deglaciation and became deeper afterwards. Paleoproductivity increase at LGM~16 ka BP was caused by the Australian-Indonesian winter monsoon (AIWM)-like condition, characterised by intense coastal upwelling while the Holocene paleoproductivity increase was related to the abrupt rainfall increase which enhanced terrestrial/riverine input. Thermocline depth variability in the western Savu Strait is in-phase with thermocline depth variability in the Java upwelling region, characterised by a shallower thermocline during the LGM–Last Deglaciation (before ~11.65 ka BP) and a deeper thermocline during the Holocene (after ~11.65 ka BP). This thermocline depth shifting indicates a strong Australian-Indonesian Monsoon (AIM) influence on the paleoceanography of the western Savu Strait since LGM.

Keywords:

Australian-Indonesian monsoon; foraminiferal accumulation rate; Indonesian Throughflow; paleoproductivity; Savu Strait

1. Introduction

Sea surface paleoproductivity is one of the key elements in paleoclimate and paleoceanographic studies as it is part of the carbon cycle, the crucial driver behind the climatic changes throughout the Earth's history (Kump et al., 2004). Relative changes in sea surface paleoproductivity (simplified as paleoproductivity in the next part of the article) are driven by nutrient availability on the surface and near-surface of seawater mass known as the photic zone (Brasier, 1995). One mechanism that causes nutrient availability to increase in the photic zone is the uplifting of the nutrient-rich cool water layer to the photic zone, known as upwelling (Brasier, 1995; Susanto et al., 2001). In addition to upwelling, increasing riverine/terrestrial input due to rainfall enhancement or the opening of a new seaway could also intensify the

nutrient availability in the photic zone (Setiawan et al., 2015; Xu et al., 2017).

Since the Last Glacial Maximum (LGM), two distinct mechanisms could be detected from the paleoproductivity changes in the Southern Indonesia seas. In the Java upwelling region, which is situated along the southern coast of Sumatra, Java, and the western Lesser Sunda Islands, paleoproductivity enhancement before Holocene was accompanied by a thermocline depth shoaling (Spooner et al., 2005; Mohtadi et al., 2011). This thermocline depth shoaling was related to the upwelling intensification due to Australian-Indonesian winter monsoon (AIWM) enhancement (Spooner et al., 2005; Mohtadi et al., 2011; Ardi et al., 2021). A different mechanism occurred in the Timor Sea, the main passage of the Indonesian Throughflow (ITF) as the LGM–Last Deglaciation paleoproductivity enhancement was not accompanied by thermocline depth shoaling (Xu et al., 2008; Holbourn et al., 2011). The increase of paleoproductivity in the ITF outflow region during this period

Corresponding author: Ryan Dwi Wahyu Ardi

e-mail address: dwa.ryan@students.itb.ac.id; dwa.ryan@gmail.com

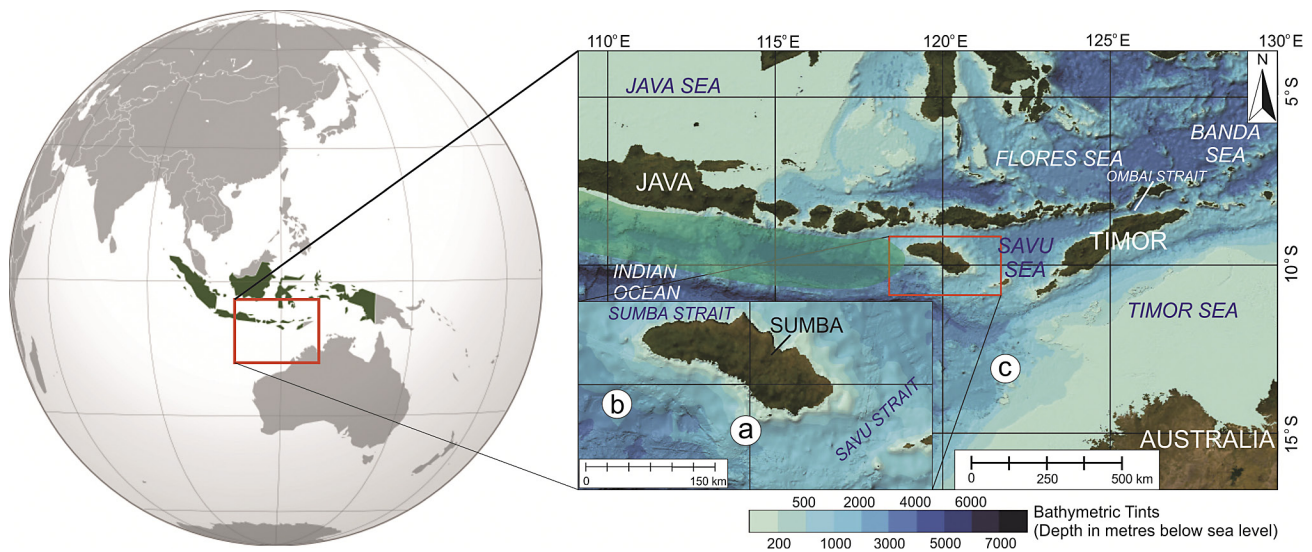


Figure 1: Locations of gravity core ST10 for this study (a), gravity core ST08 of Ardi et al. (2021), and core MD01-2378 studied by Xu et al. (2008) and Holbourn et al. (2011) (c). Green shading indicates the Java upwelling region. Bathymetric data (right figure) were obtained from GEBCO Bathymetric Compilation Group 2020 (2020), and the globe figure (left figure) was obtained from [https://en.wikipedia.org/wiki/File:Indonesia_\(orthographic_projection\).svg](https://en.wikipedia.org/wiki/File:Indonesia_(orthographic_projection).svg).

could be related to the increase in terrestrial input due to the exposure of the Sahul Shelf (Holbourn et al., 2005; Lo Giudice Cappelli et al., 2016).

A previous study on Sumba Island offshore (off Southwest Sumba and Sumba Strait) (see b in Figure 1) found that the paleoproductivity changes in this area were similar to the Java upwelling region, which was higher during LGM–Last Deglaciation due to the AIWM-induced *upwelling intensification* (Ardi et al., 2021). That study, however, did not cover the Savu Strait, which is part of the minor ITF outflow passage (branched from the Ombai Strait passage, Figure 2) along with the Sumba Strait. A recent oceanographic study indicated that a larger ITF outflow could pass the Savu Strait passage in comparison to the Sumba Strait passage (~0.1 Sv) (Bayhaqi et al., 2019), indicating a greater ITF influence on the oceanography of the Savu Strait. A similar condition might occur during LGM–Last Deglaciation in the Savu Strait hence its mechanism of paleoproductivity changes could be related to the increase in terrestrial input caused by the exposure of the Sahul Shelf, similar to the main ITF outflow region (the Timor Sea) (Holbourn et al., 2005; Lo Giudice Cappelli et al., 2016). This research uses foraminiferal accumulation rate of gravity core ST10 from off the South Sumba, situated in the western Savu Strait (see Figure 1) to confirm the mechanism of paleoproductivity changes around the Savu Strait passage. Paleoproductivity discussed in this study, is the amount of biogenic materials produced in the near sea surface water layer (photic zone) (Kump et al., 2004). One of the potential proxies to infer relative paleoproductivity changes are microfossils found in deep sea sediments. Various microfossils have been widely applied through their abundances and accumulation rate, i.e. calcareous nan-

nofossils (e.g. Andrulleit et al., 2008), foraminifera (e.g. Spooner et al., 2005; Ardi et al., 2021), dinoflagellates (e.g. Murgese et al., 2008), and diatoms (e.g. Romero et al., 2012).

2. Regional Climate and Oceanography

Australian-Indonesian monsoon (AIM) and ITF dominantly shape the oceanography of the Indonesian seas (Gordon, 2005; Ding et al., 2013; Sprintall and Réveillard, 2014). AIM consists of two phases that switch bi-annually, Australian-Indonesian summer monsoon (AISM) (December–March) and AIWM (April–September) due to the latitudinal shifts of the Inter-tropical Convergence Zone (ITCZ) (Wheeler and McBride, 2005; Wang et al., 2017). During AISM, ITCZ lies around Northern Australia (Austral summer ITCZ) hence the northwest winds carry moist air from the South China Sea to Indonesia, triggering the wet season (Wheeler and McBride, 2005). The dry season occurs during AIWM when the dry southeast winds pass through the Indonesian archipelago, and the ITCZ lies around Indochina (Austral winter ITCZ) (Wheeler and McBride, 2005) (see Figure 2). The AIM influence is the most salient in the Southern Indonesian region, where the difference between the dry and wet season rainfall is the highest (Aldrian and Susanto, 2003). This bi-annual shift of AIM phases affects the vertical profile of the ITF and the flow direction of several seasonal currents in Indonesian seas such as the Karimata Strait Throughflow (KSTF), the South Java Current (SJC), and the Leeuwin Current (LC) (Gordon, 2005; Qu et al., 2005).

KSTF flows to the southeast during the AISM, delivering warm and fresh surface waters to the southern edge of the Makassar Strait and the Flores Sea (Qu et al.,

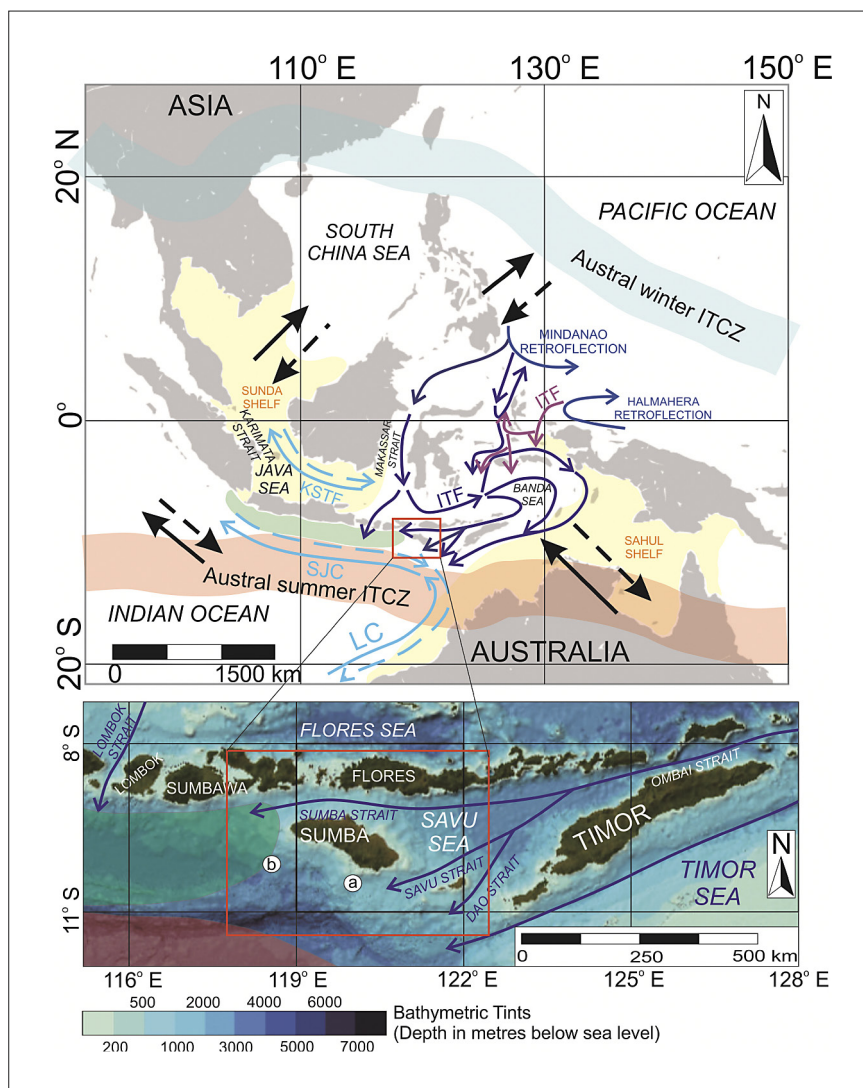


Figure 2: The regional climate and oceanography of Indonesia adapted from several authors (Gordon, 2005; Qu et al., 2005; Andruleit et al., 2008; Mohtadi et al., 2009; Sprintall et al., 2009; Kuhnt et al., 2015; Di Nezio et al., 2016; Wang et al., 2017; Bayhaqi et al., 2019). The red-outlined rectangular indicates the study area, the white circles indicate the location of gravity core ST10 (a) (this study) and ST08 (Ardi et al., 2021) (b), the blue arrows indicate the route of ITF with North Pacific water mass, the purple arrows indicate the route of ITF with South Pacific water mass, the cyan arrows indicate the seasonally reversed currents (SJC, KSTF, and LC) (dashed: during AISM; normal: during AIWM), the green shading indicates the Java upwelling region, the light blue shading indicates the Austral winter ITCZ, the red shading indicates the Austral summer ITCZ, and the yellow shading indicates the Sunda and Sahul shelves. Bathymetric data (bottom figure) were obtained from GEBCO Bathymetric Compilation Group 2020 (2020).

2005; Gordon et al., 2012). At this time, thermocline depth shoaling occurs in the ITF exit passage due to the obstruction of ITF surface flow by these water masses, forming the thermocline-dominated ITF (Tomczak and Godfrey, 2003; Qu et al., 2005). KSTF flows northwest during AIWM hence the ITF surface flow could reach the ITF exit passage, triggering thermocline depth deepening (Tomczak and Godfrey, 2003; Qu et al., 2005). SJC flows northwest while being fed by the nutrient-rich northward flow of LC during AIWM, forming the coastal upwelling along the western part of Southern Indonesia seas known as the Java upwelling region (Susanto et al., 2001; Ningsih et al., 2013) (see Figure 2). This

coastal upwelling is absent during the AISM as the SJC flows southeast and feeds the southward flow of LC (Tomczak and Godfrey, 2003; Gordon, 2005).

ITF is part of the global thermohaline circulation and the only inter-ocean flow in tropical region (Gordon, 1986, 2005; Tomczak and Godfrey, 2003). ITF water masses flowing from Mindanao retroflection (composed of the North Pacific water mass) and Halmahera retroflection (composed of the South Pacific water mass) (Gordon, 2005; Sprintall et al., 2014). ITF water mass exits the Indonesian archipelago and flows to the Indian Ocean through three different passages i.e. the Timor Sea (~7.5 Sv; the main passage), the Lombok Strait

Table 1: Gravity core ST10 information

Core	Location	Coordinate		Depth (metres below sea level)	Length (cm)
		Longitude (°E)	Latitude (°S)		
ST10	Off South Sumba (western Savu Strait)	119.885	10.491	1004	137

(~2.6 Sv), and the Ombai Strait (~4.9 Sv) (**Sprintall et al., 2009**) (see **Figure 2**). The Ombai Strait passage branches into three passages, two of which encircle Sumba Island (Sumba Strait and Savu Strait) (**Potemra, 2003; Sprintall et al., 2009**). Most of the Ombai Strait outflow passes through the Savu Strait and Dao Strait (~4.8 Sv) while the Sumba Strait is only passed by a minor transport of ITF (~0.1 Sv) (**Bayhaqi et al., 2019**).

3. Material and Methods

Gravity core ST10 was collected during the 2016 Widya Nusantara Expedition (E-WIN) from off South Sumba, western Savu Strait (see **Figures 1 and 2, Table 1**). The sub-samples for foraminiferal determination were taken at 2 cm intervals, resulting in a total of 69 sub-samples. Sub-samples were weighed to ensure the weight consistency for each sub-sample (~5 g) and dried in a drying oven for ~6–8 hours at 40°C afterwards. The dried sub-samples were then carefully mashed and stored in a measurement tube to measure their volume. The sub-samples were weighed again before being washed on the top of a 230 mesh (63 µm) sieve to separate the foraminiferal specimens from mud. After the mud was gone, the residue was dried in a drying oven for ~6 hours at 60°C.

Dry samples were then sieved with 150 µm sieving. Foraminiferal analysis was carried out from >150 µm size fraction in order to exclude juvenile specimens. About 300 specimens were picked from each sample, because, according to **Dennison and Hay (1967)**, counting 300 specimens is considered enough to represent the whole species that might occur within a sample. In case of large sample volumes, we split each sample several times until it contains only ~300 specimens of foraminifera. Afterwards, each species number counted within each sample will be multiplied by the split number, then divided by its dry weight to get the assemblage in 1 g. Quantitative determination of foraminiferal taxa was carried out based on foraminiferal descriptions from **Kenneth and Srinivasan (1983)** and **Bolli and Saunders (1985)** as references. The identified foraminiferal taxa from quantitative determination were presented in **Supplementary Material 1**. Sample preparation and determination were conducted at the Sedimentary Laboratory of the Research Centre for Geological Disaster of the National Research and Innovation Agency (BRIN) and the Micropaleontology Laboratory of Institut Teknologi Bandung (ITB).

Geochronology of ST10 was made following the Bayesian age-modelling using the rbacon package in R (version 2.4.2). The age-model reconstruction was derived from two Accelerator Mass Spectrometry (AMS) ¹⁴C dating (interval 40–41 cm and 136–137 cm), analysed on the planktonic foraminiferal shells (*Neogloboquadrina* spp.). The analysis was conducted in Beta Analytic Inc. (Beta), USA, and Woods Hole Oceanographic Institution, USA (OS). The obtained radiocarbon age was converted to calibrated calendar ages with the High Probability Density Range (HPD) Method (**Bronk Ramsey, 2009**) using the MARINE13 calibration datasets (**Reimer et al., 2013**) as reference with a reservoir correction (ΔR) of 51 ± 87 years. Since the sediment core ST10 was collected in 2016 and the reference present time is 1950 AD (**Currie, 2004**), the core top age will be –66 BP. The AMS ¹⁴C Calendar Age was combined with the age of Younger Dryas onset obtained from the correlation between *Globigerinoides* (*Gs.*) *ruber* oxygen isotope (δ¹⁸O) records of core ST10 (see **Supplementary Material 2**) and NGRIP GICC05 (North Greenland Ice Core Project, Greenland Ice Core Chronology 2005) δ¹⁸O records (reference present time = 1950 AD) (**Andersen et al., 2007**). For AMS ¹⁴C dates, approximately 250–300 specimens of planktonic foraminifera *Neogloboquadrina* spp. were picked from >250 µm size fraction. Furthermore, about ~6 specimens of *Gs. ruber* were also picked from 250–350 µm size fraction for oxygen isotope (δ¹⁸O) analysis material. The δ¹⁸O analysis was conducted in the Benedum Stable Isotope Laboratory of Brown University, USA.

Foraminiferal Accumulation Rate (FAR) and Benthic Foraminiferal Accumulation Rate (BFAR) (the number of specimens per cm² sea floor per ka) were used to infer the relative paleoproductivity changes (**Ehrmann and Thiede, 1986; Dürkop et al., 2008**) (see **Supplementary Material 3**). These proxies were widely applied to paleoproductivity studies based on foraminiferal occurrence in marine sediment (**Herguera, 2000; Murgese et al., 2008; Nagai et al., 2010; Garcia et al., 2013**). The formula to calculate FAR and BFAR is written in **Equation 1** and **Equation 2** (**Ehrmann and Thiede, 1986**) as follows:

$$\text{FAR (specimens/cm}^2\text{/ka)} = \text{foraminiferal specimens (/gram)} \times \text{AR}_{\text{BULK}} \quad (1)$$

Where:

Bulk accumulation rate (AR_{BULK}) (g/cm² ka) – linear sedimentation rates (cm/ka) × DBD,
DBD – Dry Bulk Density (g/cm³).

BFAR (specimens/cm²/ka) = benthic foraminiferal specimens (/gram) × AR_{BULK} (2)

Where:

Bulk accumulation rate (AR_{BULK}) (g/cm² ka) – linear sedimentation rates (cm/ka) × DBD,

DBD – Dry Bulk Density (g/cm³).

DBD can be calculated using Equation 3 (Ehrmann and Thiede, 1986) as follows:

$$DBD = \frac{\text{sediment weight (g)}}{\text{sediment volume (cm}^3\text{)}} \quad (3)$$

Paleoproductivity reconstruction derived from FAR and BFAR was correlated to the thermocline depth variability, which was inferred from the relative abundances of thermocline dwellers taxa (i.e. *Neogloboquadrina dutertrei*, *Pulleniatina obliqueloculata*, and *Globorotalia menardii*) (see Supplementary Material 4) to analyse the mechanism of paleoproductivity changes. The shoal-

ing of thermocline depth was indicated by the increase of thermocline dwellers' abundance while thermocline depth deepening was indicated by the thermocline dwellers' abundance decrease (Bé et al., 1977; Ravelo et al., 1990; Spooner et al., 2005; Maryunani, 2009; Ding et al., 2013; Steinke et al., 2014b)

4. Results and Discussion

AMS ¹⁴C dating analysis from 2 samples reveals the Calendar age of 13850 ± 55 for depth intervals of 40–41 cm and 33280 ± 200 for depth intervals of 136–137 cm (see Table 2). The tie point between *Gs. ruber* δ¹⁸O with that of NGRIP GICC05 δ¹⁸O (Andersen et al., 2007) demonstrates the Younger Dryas onset at interval 32–33 cm, which indicates 12570 ± 129 BP (see Figure 3, Table 3). Age model reconstruction was then conducted by using the Bayesian age-modelling (ver. 2.4.2), which resulted in an abrupt sedimentation rate decrease at ~40

Table 2: AMS ¹⁴C ages and calibrated AMS ¹⁴C ages of core ST10, analysed in Beta Analytic Inc. (Beta), USA and Woods Hole Oceanographic Institution, USA (OS)

Lab code	Core	Depth intervals	Materials	¹⁴ C age (BP)	Calibrated ¹⁴ C age BP
OS-169053	ST10	40–41 cm	Foraminifera: <i>Neogloboquadrina</i> spp.	13850 ± 55	16533–15553
Beta-572243	ST10	136–137 cm	Foraminifera: <i>Neogloboquadrina</i> spp.	33280 ± 200	35721–34286

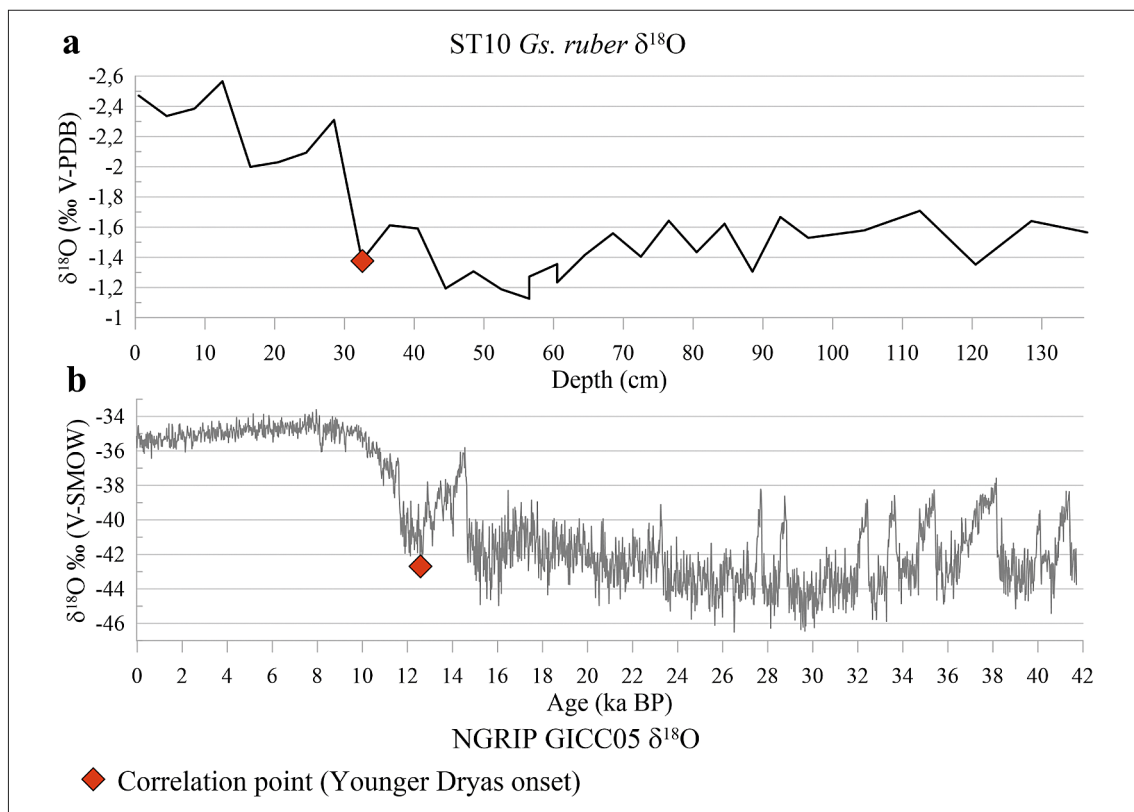


Figure 3: Correlation between (a) *Gs. ruber* δ¹⁸O records of core ST 10. and (b) NGRIP GICC05 δ¹⁸O records (reference present time = 1950 AD) (Andersen et al., 2007). Red diamonds indicate the correlation point (Younger Dryas onset).

Table 3: Detailed information about the age of Younger Dryas onset obtained from the correlation between *Gs. ruber* $\delta^{18}\text{O}$ records of core ST10 and NGRIP GICC05 $\delta^{18}\text{O}$ records (reference present time = 1950 AD) (Andersen et al., 2007)

Event	Core	Depth intervals	Methods	GICC05 age (BP)
Younger Dryas onset	ST10	32–33 cm	<i>Gs. ruber</i> $\delta^{18}\text{O}$	12570 \pm 129

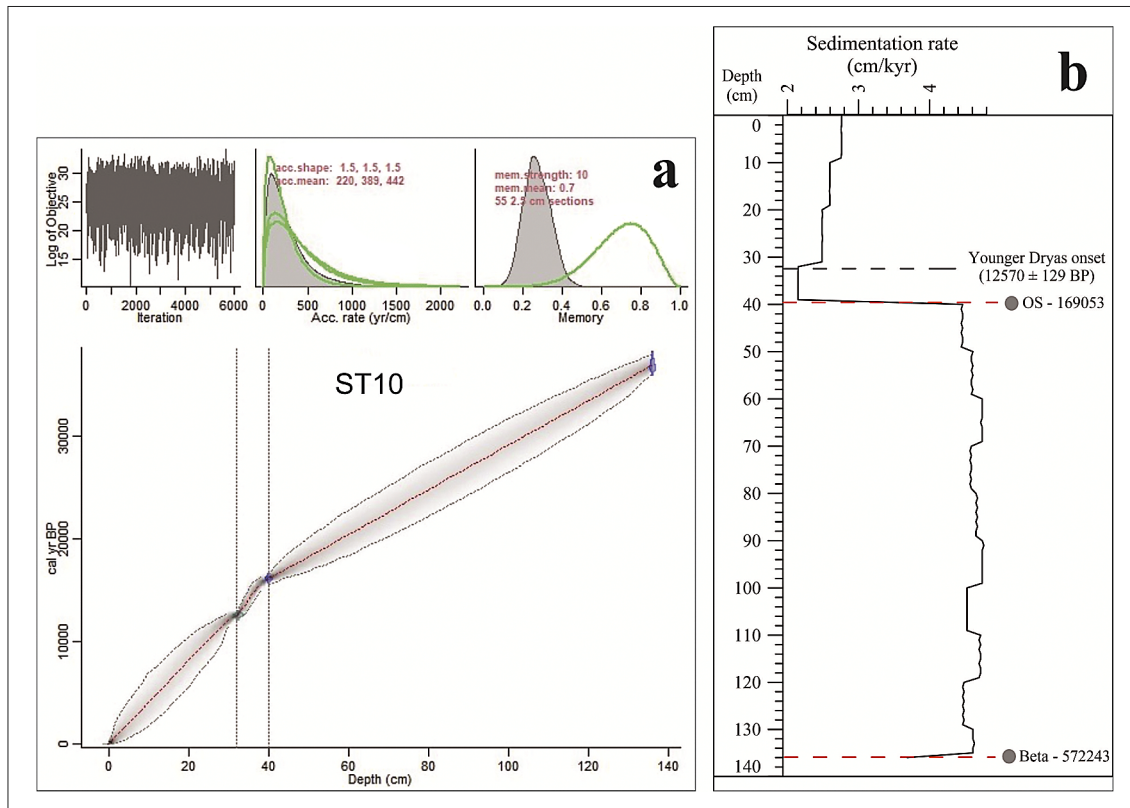


Figure 4: (a) Bayesian age model (Blaauw and Christen, 2011) of core ST10 using rbacon package (version 2.4.2) (Blaauw et al., 2020) in R (R Core Team, 2013). The upper panels depict the Markov chain Monte Carlo (MCMC) iterations (left panel), the prior (green curves) and posterior (grey histograms) distributions for the accumulation rate (middle panel), and memory (right panel) (Blaauw et al., 2020). The bottom panel shows the calibrated ^{14}C dates (transparent blue) and the age-depth model (darker greys indicate more likely calendar ages, grey stippled lines show 95% confidence intervals, and red lines indicate a single 'best' model based on the mean ages) (Blaauw et al., 2020). (b) Sedimentation rates of core ST10 obtained from the Bayesian age model.

cm depth and a slight sedimentation rate increase from ~30 cm depth upward (see Figure 4). This research will be focused on the top 77 cm of core ST10 which represents about the last 23 kilo-annum (ka) (LGM–Holocene) time.

FAR was relatively higher before ~16 ka BP ($\sim 44 \times 10^3$ specimens/cm²/ka on average) and after ~11.65 ka BP (Holocene) ($\sim 36 \times 10^3$ specimens/cm²/ka on average). FAR gradually decreased during LGM—~19 ka BP (from $\sim 64 \times 10^3$ to $\sim 40 \times 10^3$ specimens/cm²/ka) and abruptly declined after ~16 ka BP (from $\sim 40 \times 10^3$ to $\sim 16 \times 10^3$ specimens/cm²/ka). At the beginning of the Holocene, FAR gradually increased until ~5.5 ka BP (from $\sim 26 \times 10^3$ to $\sim 52 \times 10^3$ specimens/cm²/ka) and gradually declined afterwards (from $\sim 52 \times 10^3$ to $\sim 20 \times 10^3$ specimens/cm²/ka) (see Figure 5a). Similar trends were also detected on BFAR with higher values indicated before ~16 ka BP ($\sim 2 \times 10^3$ specimens/cm²/ka on av-

erage) and during the Holocene ($\sim 1.6 \times 10^3$ specimens/cm²/ka on average) (see Figure 5b). Thermocline dwellers were relatively higher ($\sim 42\%$ on average) during the LGM–Last Deglaciation (before ~11.65 ka BP) with a less prominent increase before ~16 ka BP ($\sim 46\%$ on average) (see Figure 5c). During the Holocene (after ~11.65 ka BP), thermocline dwellers indicated a contrast pattern to FAR and BFAR which was decreasing ($\sim 36\%$ on average). In general, FAR and BFAR increase during LGM—~16 ka BP was accompanied by thermocline shoaling while the Holocene FAR and BFAR increase was in phase with thermocline deepening (see Figure 5a–c). Based on the FAR and BFAR changes, paleoproductivity was relatively higher before ~16 ka BP (FAR: $\sim 44 \times 10^3$ specimens/cm²/ka on average; BFAR: $\sim 2 \times 10^3$ specimens/cm²/ka on average) and during the Holocene (FAR: $\sim 36 \times 10^3$ specimens/cm²/ka on average; BFAR: $\sim 1.6 \times 10^3$ specimens/cm²/ka on average) in

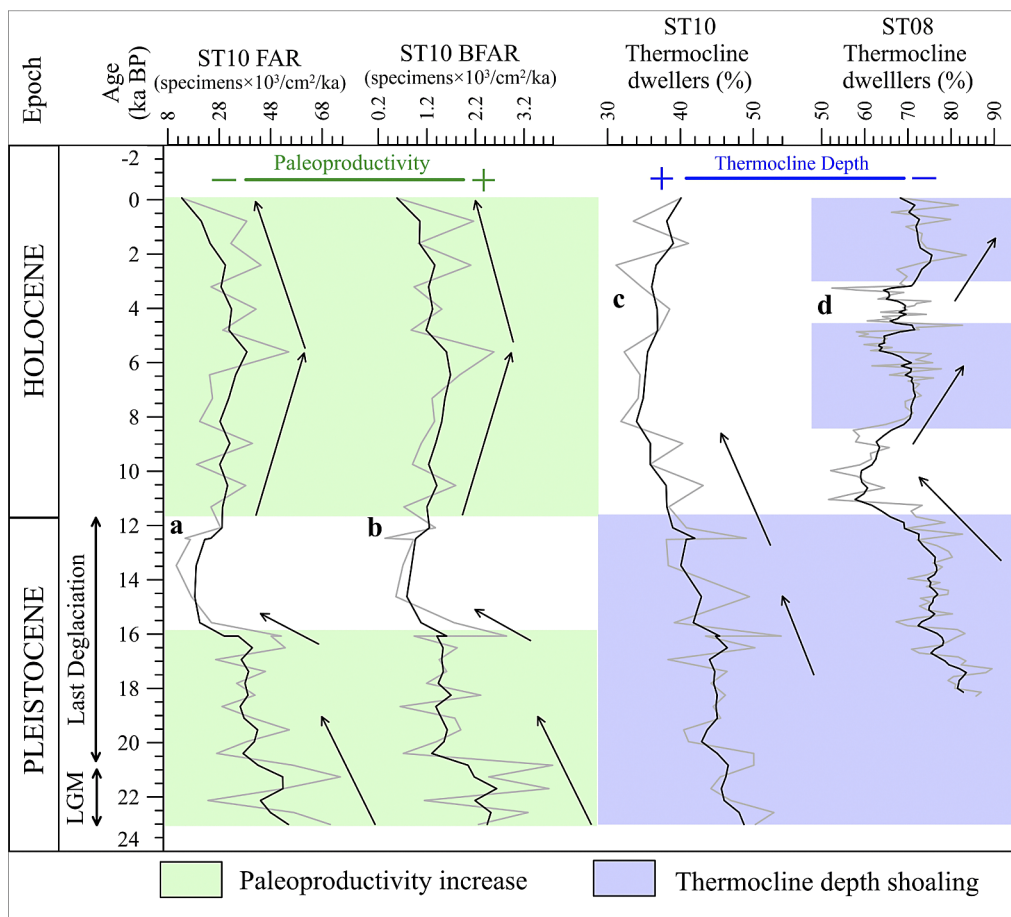


Figure 5: Paleoproductivity (a and b) and thermocline depth proxies of core ST10 (c) compared to thermocline depth proxy of core ST08 (Ardi et al., 2021) (d). Black curves indicate smoothed values (exponential smoothing damping factor 0.7). Pleistocene–Holocene boundary = 11.653 ± 99 BP (Rasmussen et al., 2006).

comparison to ~ 16 – 11.65 ka BP (FAR: $\sim 16 \times 10^3$ specimens/cm²/ka on average; BFAR: $\sim 0.8 \times 10^3$ specimens/cm²/ka on average) (see Figure 5a–b). A higher abundance of thermocline dwellers during the LGM–Last Deglaciation ($\sim 42\%$) indicated thermocline shoaling while lower thermocline dwellers abundance during the Holocene ($\sim 36\%$ on average) indicated thermocline deepening (see Figure 5c). A slightly higher thermocline dwellers’ abundance before ~ 16 ka ($\sim 46\%$ on average) might also indicate a shallower thermocline depth compared to ~ 16 – 11.65 ka BP (see Figure 5c).

Thermocline depth in core ST10 (western Savu Strait) was shoaling during LGM–Last Deglaciation, derived from the increasing thermocline dwellers’ abundance (see Figure 5c). This condition is in phase with the thermocline depth record from the nearby location (ST08) (see Figure 5d) which is located within the Java upwelling regime (Ardi et al., 2021). According to previous studies (Spooner et al., 2005; Mohtadi et al., 2011; Ding et al., 2013; Ardi et al., 2021), the shoaling thermocline depth during this time in this region was related to the multi-millennial shifting of AIM which generated AIWM-like conditions by enhancing the coastal

upwelling in the Southern Indonesia region. The slow-down of thermohaline circulation during LGM–Last Deglaciation (Rühlemann et al., 1999; Schmidt et al., 2012) could weaken the ITF (Xu et al., 2006; Lo Giudice Cappelli et al., 2016) and invited more SJC water mass into the Savu Strait, similar to the modern condition during AIWM (Potemra, 2003; Sprintall et al., 2010).

During Mid and Late Holocene, thermocline dwellers’ abundance in the western Savu Strait was relatively lower, which indicated thermocline deepening (see Figure 5c). This occurrence was antiphase with the records from the Java upwelling regime (Ardi et al., 2021) (see Figure 5d), which demonstrated an increased pattern, suggesting shoaling thermocline depth. This denoted that the effects of Mid–Late Holocene solar activity on AIM changes that influence the Java upwelling region (Steinke et al., 2014a; Ardi et al., 2020), apparently did not affect the oceanographic condition of the western Savu Strait. In the Java upwelling region, the solar activity enhancement during Mid and Late Holocene resulted in AIWM enhancement, which induced thermocline depth shoaling (Steinke et al., 2014a).

Paleoproductivity enhancement during LGM~16 ka BP (see **Figure 5a–b**) could be related to the coastal upwelling intensification due to the in-phase relation between the western Savu Strait and Java upwelling regime thermocline depth records (see **Figure 5c–d**) which indicated thermocline depth shoaling (**Mohtadi et al., 2011; Ardi et al., 2021**). The AIWM-like condition characterised by intense coastal upwelling most likely ended at ~16 ka BP, indicated by the abrupt paleoproductivity decline (see **Figure 5a–b**). This abrupt paleoproductivity decline might have resulted from the activation of AISM ~16 – 14 ka BP, which reduced the coastal upwelling intensity (**Wyrwoll and Miller, 2001; Spooner et al., 2005**).

Paleoproductivity enhancement during the Holocene (see **Figure 5a–b**) could be associated with the increase of terrestrial/riverine materials input which enhanced the nutrient availability at surface water (**Brasier, 1995; Kawamura et al., 2006**). The terrestrial/riverine input enhancement during this time was derived from the abrupt enhancement of the Early Holocene rainfall related to the sea level rise (**Griffiths et al., 2009, 2010; Setiawan et al., 2015; Xu et al., 2017**). The Early Holocene sea level rise was able to submerge the entire Sunda and Sahul shelves which expanded the Indonesian sea surface, increasing the water vapour source for rainfall intensification (**Griffiths et al., 2009, 2010**).

Future research will be a comprehensive study of the paleoproductivity changes in both the Sumba Strait and the Savu Strait. New and improved datasets from sediment cores on both passages will be applied to generate a more robust paleoproductivity reconstruction. Qualitative models and maps of the boundary between the Java upwelling regime and the ITF outflow regime on the sea around Sumba Island are also expected.

5. Conclusions

- (1) Paleoproductivity increase was indicated in the western Savu Strait during LGM~16 ka BP and Holocene (after ~11.65 ka BP). The increase of paleoproductivity during LGM~16 ka BP which was characterised by intense coastal upwelling was due to the AIWM-like condition. While the Holocene paleoproductivity escalation was related to the abrupt rainfall increase which enhanced terrestrial/riverine input.
- (2) Thermocline depth variability in the western Savu Strait which was characterised by a shallower thermocline during the LGM–Last Deglaciation (before ~11.65 ka BP) and deeper thermocline during the Holocene (after ~11.65 ka BP) is in-phase with the thermocline depth shifting in Java upwelling regime. This pattern indicates a strong AIM influence on the thermocline depth changes off South Sumba.

Acknowledgement

This research is part of the doctoral dissertation research (contract number: 083/E5/PG.02.00.PT/2022) funded by Directorate General of Higher Education, Ministry of Education, Culture, Research, and Technology, Republic of Indonesia, granted to Aswan, Khoiril Anwar Maryunani, and Ryan Dwi Wahyu Ardi. We also thank the Research Centre for Oceanography of Indonesian Institute of Science (now BRIN), especially Udhi Hermawan, Ph.D. as the chief scientist of E-WIN 2016 for the permission of data usage and administrative assistance and all crews of the Baruna Jaya VIII R.V., especially Singgih Adi Wibowo for technical supports and data collecting. The Research Centre Geological Disaster of BRIN and Geological Engineering Department of ITB are thanked for the laboratory facilities. We also express our gratitude to the Indonesian Endowment Fund for Education (LPDP) (contract number: 2020011 10215954) for the financial assistance during Ryan Dwi Wahyu Ardi's doctoral study. Rizky Amalia Maulidiatyani is thanked for her professional proofreading.

Supplementary materials

The following supporting information can be downloaded at:

Supplementary Material 1 <https://hrcak.srce.hr/ojs/index.php/rgn/article/view/23308/13611>

Supplementary Material 2 <https://hrcak.srce.hr/ojs/index.php/rgn/article/view/23308/13612>

Supplementary Material 3 <https://hrcak.srce.hr/ojs/index.php/rgn/article/view/23308/13613>

Supplementary Material 3 <https://hrcak.srce.hr/ojs/index.php/rgn/article/view/23308/13614>

6. Abbreviations

AIM: Australian-Indonesian monsoon
 AISM: Australian-Indonesian summer monsoon
 AIWM: Australian-Indonesian winter monsoon
 AMS: Accelerator Mass Spectrometry
 BFAR: Benthic Foraminiferal Accumulation Rate
 BRIN: National Research and Innovation Agency
 E-WIN: Widya Nusantara Expedition
 FAR: Foraminiferal Accumulation Rate
 GICC05: Greenland Ice Core Chronology 2005
 HPD: High Probability Density
 ITB: Institut Teknologi Bandung
 ITCZ: Inter-tropical Convergence Zone
 ITF: Indonesian Throughflow
 KSTF: Karimata Strait Throughflow
 LC: Leeuwin Current
 LGM: Last Glacial Maximum
 NGRIP: North Greenland Ice Core Project
 SJC: South Java Current
 V-PDB: Vienna Pee Dee Belemnite
 V-SMOW: Vienna Standard Mean Ocean Water

7. References

- Aldrian, E., and Susanto, R. D. (2003): Identification of three dominant rainfall regions within Indonesia and their relationship to sea surface temperature, *International Journal of Climatology*, 23(12), 1435–1452. <https://doi.org/10.1002/joc.950>.
- Andrulleit, H., Lückge, A., Wiedicke, M., and Stäger, S. (2008): Late Quaternary development of the Java upwelling system (eastern Indian Ocean) as revealed by coccolithophores, *Marine Micropaleontology*, 69(1), 3–15. <https://doi.org/10.1016/j.marmicro.2007.11.005>.
- Ardi, R. D. W., Aswan, Maryunani, K. A., Yulianto, E., Putra, P. S., and Nugroho, S. H. (2021): Changes of thermocline depth at the Sumba Island offshore based on planktonic foraminiferal assemblages and its implication to eutrophication since the Last Deglaciation (~18 ka BP): a preliminary study, *Rudarsko-Geološko-Naftni Zbornik*, 36(3), 31–45. <https://doi.org/10.17794/rgn.2021.3.3>.
- Ardi, R. D. W., Aswan, Maryunani, K. A., Yulianto, E., Putra, P. S., Nugroho, S. H., and Istiana (2020): Last Deglaciation—Holocene Australian-Indonesian Monsoon Rainfall Changes Off Southwest Sumba, Indonesia, *Atmosphere*, 11(9), 932. <https://doi.org/10.3390/atmos11090932>.
- Bayhaqi, A., Lenn, Y.-D., Surinati, D., Polton, J., Nur, M., Corvianawatie, C., and Purwandana, A. (2019): The Variability of Indonesian Throughflow in Sumba Strait and Its Linkage to the Climate Events, *American Journal of Applied Sciences*, 16(4), 118–133. <https://doi.org/10.3844/ajassp.2019.118.133>.
- Bé, A. W. H., Hutson, W. H., and Be, A. W. H. (1977): Ecology of Planktonic Foraminifera and Biogeographic Patterns of Life and Fossil Assemblages in the Indian Ocean, *Micropaleontology*, 23(4), 369–414. <https://doi.org/10.2307/1485406>.
- Blaauw, M., and Christen, J. A. (2011): Flexible paleoclimate age-depth models using an autoregressive gamma process, *Bayesian Analysis*, 6(3), 457–474. <https://doi.org/10.1214/11-BA618>.
- Bolli, H. M., and Saunders, J. B. (1985): Oligocene to Holocene low latitude planktic foraminifera (1st ed.). In: Bolli, H. M., Saunders, J. B. and Perch-Nielsen, K. (eds.): *Plankton Stratigraphy* – Cambridge University Press, New York. 155-262, 1032 p.
- Brasier, M. D. (1995): Fossil indicators of nutrient levels. 1: eutrophication and climate change, *Marine Palaeoenvironmental Analysis from Fossils*, (83), 113–132.
- Bronk Ramsey, C. (2009): Bayesian Analysis of Radiocarbon Dates, *Radiocarbon*, 51(1), 337–360. <https://doi.org/10.1017/s003822200033865>.
- Currie, L. A. (2004): The remarkable metrological history of radiocarbon dating [II], *Journal of Research of the National Institute of Standards and Technology*, 109, 186–205.
- Dennison, J. M., and Hay, W. W. (1967): Estimating the Needed Sampling Area for Subaquatic Ecologic Studies, *Journal of Paleontology*, 41(3), 706–708.
- Di Nezio, P. N., Timmermann, A., Tierney, J. E., Jin, F., Otto-Bliesner, B., Rosenbloom, N., Mapes, B., Neale, R., Ivanovic, R. F., and Montenegro, A. (2016): The climate response of the Indo-Pacific warm pool to glacial sea level, *Paleoceanography*, 31(6), 866–894. <https://doi.org/10.1002/2015PA002890>.
- Ding, X., Bassinot, F., Guichard, F., and Fang, N. Q. (2013): Indonesian Throughflow and monsoon activity records in the Timor Sea since the last glacial maximum, *Marine Micropaleontology*, 101, 115–126. <https://doi.org/10.1016/j.marmicro.2013.02.003>.
- Dürkop, A., Holbourn, A., Kuhnt, W., Zuraida, R., Andersen, N., and Grootes, P. M. (2008): Centennial-scale climate variability in the Timor Sea during Marine Isotope Stage 3, *Marine Micropaleontology*, 66(3–4), 208–221. <https://doi.org/10.1016/j.marmicro.2007.10.002>.
- Ehrmann, W. U., and Thiede, J. (1986): Correlation of terrigenous and biogenic sediment fluxes in the North Atlantic Ocean during the past 150 my, *Geologische Rundschau*, 75(1), 43–55. <https://doi.org/10.1007/BF01770177>.
- Garcia, J., Mojtahid, M., Howa, H., Michel, E., Schiebel, R., Charbonnier, C., Anschutz, P., and Jorissen, F. J. (2013): Benthic and Planktic foraminifera as indicators of late glacial to Holocene paleoclimatic changes in a marginal environment: An example from the southeastern bay of Biscay, *Acta Protozoologica*, 52(3), 161–180. <https://doi.org/10.467/16890027AP.13.0015.1112>.
- Gordon, A. L. (1986): Interocean exchange of thermocline water, *Journal of Geophysical Research*, 91(C4), 5037. <https://doi.org/10.1029/jc091ic04p05037>.
- Gordon, A. L. (2005): Oceanography of the Indonesian Seas and Their Throughflow, *Oceanography*, 18(4), 14–27. <https://doi.org/10.5670/oceanog.2005.01>.
- Gordon, A. L., Huber, B. A., Metzger, E. J., Susanto, R. D., Hurlburt, H. E., and Adi, T. R. (2012): South China Sea throughflow impact on the Indonesian throughflow, *Geophysical Research Letters*, 39(11), 1–7. <https://doi.org/10.1029/2012GL052021>.
- Griffiths, M. L., Drysdale, R. N., Gagan, M. K., Frisia, S., Zhao, J. X., Ayliffe, L. K., Hantoro, W. S., Hellstrom, J. C., Fischer, M. J., Feng, Y. X., and Suwargadi, B. W. (2010): Evidence for Holocene changes in Australian-Indonesian monsoon rainfall from stalagmite trace element and stable isotope ratios, *Earth and Planetary Science Letters*, 292(1–2), 27–38. <https://doi.org/10.1016/j.epsl.2010.01.002>.
- Griffiths, M. L., Drysdale, R. N., Gagan, M. K., Zhao, J. X., Ayliffe, L. K., Hellstrom, J. C., Hantoro, W. S., Frisia, S., Feng, Y. X., Cartwright, I., Pierre, E. S., Fischer, M. J., and Suwargadi, B. W. (2009): Increasing Australian-Indonesian monsoon rainfall linked to early Holocene sea-level rise, *Nature Geoscience*, 2(9), 636–639. <https://doi.org/10.1038/ngeo605>.
- Herguera, J. C. (2000): Last glacial paleoproductivity patterns in the eastern equatorial Pacific: Benthic foraminifera records, *Marine Micropaleontology*, 40(3), 259–275. [https://doi.org/10.1016/S0377-8398\(00\)00041-4](https://doi.org/10.1016/S0377-8398(00)00041-4).
- Holbourn, A., Kuhnt, W., Kawamura, H., Jian, Z., Grootes, P., Erlenkeuser, H., and Xu, J. (2005): Orbitally paced paleoproductivity variations in the Timor Sea and Indonesian throughflow variability during the last 460 kyr,

- Paleoceanography, 20(3), 1–18. <https://doi.org/10.1029/2004PA001094>.
- Holbourn, A., Kuhnt, W., and Xu, J. (2011): Indonesian Throughflow variability during the last 140 ka: The timor sea outflow, Geological Society Special Publication, 355, 283–303. <https://doi.org/10.1144/SP355.14>.
- Kawamura, H., Holbourn, A., and Kuhnt, W. (2006): Climate variability and land-ocean interactions in the Indo Pacific Warm Pool: A 460-ka palynological and organic geochemical record from the Timor Sea, Marine Micropaleontology, 59(1), 1–14. <https://doi.org/10.1016/j.marmicro.2005.09.001>.
- Kuhnt, W., Holbourn, A., Xu, J., Opdyke, B., De Deckker, P., Röhl, U., and Mudelsee, M. (2015): Southern Hemisphere control on Australian monsoon variability during the late deglaciation and Holocene, Nature Communications, 6(1), 1–7. <https://doi.org/10.1038/ncomms6916>.
- Lo Giudice Cappelli, E., Holbourn, A., Kuhnt, W., and Regenberg, M. (2016): Changes in Timor Strait hydrology and thermocline structure during the past 130 ka, Palaeogeography, Palaeoclimatology, Palaeoecology, 462, 112–124. <https://doi.org/10.1016/j.palaeo.2016.09.010>.
- Kump, L. R., Kasting, J. F., and Crane, R. G. (2004): *The Earth System* (2nd ed.), Pearson Education, Inc., New Jersey, 407 p.
- Maryunani (2009): Microfossil approach based on Cendra-wasih Bay data, to interpreting and reconstructing Equatorial Western Pacific paleoclimate since Last Glacial (Late Pleistocene). Institut Teknologi Bandung, 141 p.
- Mohtadi, M., Oppo, D. W., Steinke, S., Stuut, J. B. W., De Pol-Holz, R., Hebbeln, D., and Lückge, A. (2011): Glacial to Holocene swings of the Australian-Indonesian monsoon, Nature Geoscience, 4(8), 540–544. <https://doi.org/10.1038/ngeo1209>.
- Mohtadi, M., Steinke, S., Groeneveld, J., Fink, H. G., Rixen, T., Hebbeln, D., Donner, B., and Herunadi, B. (2009): Low-latitude control on seasonal and interannual changes in planktonic foraminiferal flux and shell geochemistry off south Java: A sediment trap study, Paleoceanography, 24(1), 1–20. <https://doi.org/10.1029/2008PA001636>.
- Murgese, D. S., De Deckker, P., Spooner, M. I., and Young, M. (2008): A 35,000 year record of changes in the eastern Indian Ocean offshore Sumatra, Palaeogeography, Palaeoclimatology, Palaeoecology, 265(3–4), 195–213. <https://doi.org/10.1016/j.palaeo.2008.06.001>.
- Nagai, R. H., Sousa, S. H. de M. e, Lourenço, R. A., Bicego, M. C., and Mahiques, M. M. De (2010): Paleoproductivity changes during the Late Quaternary in the southeastern Brazilian upper continental margin of the Southwestern Atlantic, Brazilian Journal of Oceanography, 58(spe1), 31–41. <https://doi.org/10.1590/S1679-87592010000500004>.
- Ningsih, N. S., Rakhmaputeri, N., and Harto, A. B. (2013): Upwelling variability along the southern coast of Bali and in Nusa Tenggara waters, Ocean Science Journal, 48(1), 49–57. <https://doi.org/10.1007/s12601-013-0004-3>.
- Potemra, J. T. (2003): Observed estimates of convergence in the Savu Sea, Indonesia, Journal of Geophysical Research, 108(C1), 1–11. <https://doi.org/10.1029/2002JC001507>.
- Qu, T., Du, Y., Strachan, J., Meyers, G., and Slingo, J. (2005): Sea Surface Temperature and Its Variability in the Indonesian Region, Oceanography, 18(4), 50–61. <https://doi.org/10.5670/oceanog.2005.05>.
- R Core Team (2013): A Language and Environment for Statistical Computing, R Foundation for Statistical Computing, R Foundation for Statistical Computing, Vienna, Austria, retrieved from internet: <http://www.r-project.org>.
- Rasmussen, S. O., Andersen, K. K., Svensson, A. M., Steffensen, J. P., Vinther, B. M., Clausen, H. B., Siggaard-Andersen, M.-L., Johnsen, S. J., Larsen, L. B., Dahl-Jensen, D., Bigler, M., Röthlisberger, R., Fischer, H., Goto-Azuma, K., Hansson, M. E., and Ruth, U. (2006): A new Greenland ice core chronology for the last glacial termination, Journal of Geophysical Research, 111(D6), 1–16. <https://doi.org/10.1029/2005JD006079>.
- Ravelo, A. C., Fairbanks, R. G., and Philander, S. G. H. (1990): Reconstructing Tropical Atlantic hydrography using planktonic foraminifera and an ocean model, Paleoceanography, 5(3), 409–431.
- Reimer, P. J., Edouard Bard, B., Alex Bayliss, B., Warren Beck, B. J., Paul Blackwell, B. G., and Christopher Bronk Ramsey, B. (2013): Intcal13 and Marine13 Radiocarbon Age Calibration Curves 0–50,000 Years Cal Bp, Radiocarbon, 55(4), 1869–1887. <https://doi.org/10.1017/S0033822200048864>.
- Romero, O. E., Mohtadi, M., Helmke, P., and Hebbeln, D. (2012): High interglacial diatom paleoproductivity in the westernmost Indo-Pacific Warm Pool during the past 130,000 years, Paleoceanography, 27(3), 1–14. <https://doi.org/10.1029/2012PA002299>.
- Rühlemann, C., Mulitza, S., Müller, P. J., Wefer, G., and Zahn, R. (1999): Warming of the tropical Atlantic Ocean and slowdown of thermohaline circulation during the last deglaciation, Nature, 402(6761), 511–514. <https://doi.org/10.1038/990069>.
- Schmidt, M. W., Chang, P., Hertzberg, J. E., Them, T. R., Ji, L., and Otto-Bliesner, B. L. (2012): Impact of abrupt deglacial climate change on tropical Atlantic subsurface temperatures, Proceedings of the National Academy of Sciences, 109(36), 14348–14352. <https://doi.org/10.1073/pnas.1207806109>.
- Setiawan, R. Y., Mohtadi, M., Southon, J., Groeneveld, J., Steinke, S., and Hebbeln, D. (2015): The consequences of opening the Sunda Strait on the hydrography of the eastern tropical Indian Ocean, Paleoceanography, 30(10), 1358–1372. <https://doi.org/10.1002/2015PA002802>.
- Spooner, M. I., Barrows, T. T., De Deckker, P., and Paterne, M. (2005): Palaeoceanography of the Banda Sea, and Late Pleistocene initiation of the Northwest Monsoon, Global and Planetary Change, 49(1–2), 28–46. <https://doi.org/10.1016/j.gloplacha.2005.05.002>.
- Sprintall, J., Gordon, A. L., Koch-Larrouy, A., Lee, T., Potemra, J. T., Pujiana, K., and Wijffels, S. E. (2014): The Indonesian seas and their role in the coupled ocean–climate system, Nature Geoscience, 7(7), 487–492. <https://doi.org/10.1038/ngeo2188>.
- Sprintall, J., and Révelard, A. (2014): The Indonesian Throughflow response to Indo-Pacific climate variability, Journal

- of Geophysical Research: Oceans, 119(2), 1161–1175. <https://doi.org/10.1002/2013JC009533>.
- Sprintall, J., Wijffels, S. E., Molcard, R., and Jaya, I. (2009): Direct estimates of the Indonesian throughflow entering the Indian Ocean: 2004–2006, *Journal of Geophysical Research: Oceans*, 114(7), 2004–2006. <https://doi.org/10.1029/2008JC005257>.
- Sprintall, J., Wijffels, S., Molcard, R., and Jaya, I. (2010): Direct evidence of the South Java Current system in Ombai Strait, *Dynamics of Atmospheres and Oceans*, 50(2), 140–156. <https://doi.org/10.1016/j.dynatmoce.2010.02.006>.
- Steinke, S., Mohtadi, M., Prange, M., Varma, V., Pittauerova, D., and Fischer, H. W. (2014a): Mid- to Late-Holocene Australian-Indonesian summer monsoon variability, *Quaternary Science Reviews*, 93, 142–154. <https://doi.org/10.1016/j.quascirev.2014.04.006>.
- Steinke, S., Prange, M., Feist, C., Groeneveld, J., and Mohtadi, M. (2014b): Upwelling variability off southern Indonesia over the past two millennia, *Geophysical Research Letters*, 41(21), 7684–7693. <https://doi.org/10.1002/2014GL061450>.
- Susanto, R. D., Gordon, A. L., and Zheng, Q. (2001): Upwelling along the coasts of Java and Sumatra and its relation to ENSO, *Geophysical Research Letters*, 28(8), 1599–1602. <https://doi.org/10.1029/2000GL011844>.
- Tomczak, M., and Godfrey, J. S. (2003): Adjacent seas of the Indian Ocean and the Australasian Mediterranean Sea (The Indonesian Throughflow). In: Tomczak, M., and Godfrey, J. S.: *Regional Oceanography: An Introduction*, Daya Publishing House, Delhi. 215–228, 382 p.
- Wang, P. X., Wang, B., Cheng, H., Fasullo, J., Guo, Z., Kiefer, T., and Liu, Z. (2017): The global monsoon across time scales: Mechanisms and outstanding issues, *Earth-Science Reviews*, 174(July 2016), 84–121. <https://doi.org/10.1016/j.earscirev.2017.07.006>.
- Wheeler, M. C., and McBride, J. L. (2005): Australian-Indonesian monsoon. In: Lau, W. K. M. and Waliser, D. E.: *Intra-seasonal Variability in the Atmosphere-Ocean Climate System*, Springer Berlin Heidelberg, Berlin, Heidelberg. 125–173, 477 p. https://doi.org/10.1007/3-540-27250-X_5.
- Wyrwoll, K. H., and Miller, G. H. (2001): Initiation of the Australian summer monsoon 14,000 years ago, *Quaternary International*, 82(85), 119–128. [https://doi.org/10.1016/S1040-6182\(01\)00034-9](https://doi.org/10.1016/S1040-6182(01)00034-9).
- Xu, J., Holbourn, A., Kuhnt, W., Jian, Z., and Kawamura, H. (2008): Changes in the thermocline structure of the Indonesian outflow during Terminations I and II, *Earth and Planetary Science Letters*, 273(1–2), 152–162. <https://doi.org/10.1016/j.epsl.2008.06.029>.
- Xu, J., Kuhnt, W., Holbourn, A., Andersen, N., and Bartoli, G. (2006): Changes in the vertical profile of Indonesian Throughflow during Termination II: Evidence from the Timor Sea, *Paleoceanography*, 21(4), 1–14. <https://doi.org/10.1029/2006PA001278>.
- Xu, Y., Wang, L., Yin, X., Ye, X., Li, D., Liu, S., Shi, X., Troa, R. A., Zuraida, R., Triarso, E., and Hendrizon, M. (2017): The influence of the Sunda Strait opening on paleoenvironmental changes in the eastern Indian Ocean, *Journal of Asian Earth Sciences*, 146, 402–411. <https://doi.org/10.1016/j.jseas.2017.06.014>.

SAŽETAK

Rekonstrukcija paleoproduktivnosti temeljem taloženja foraminifera u zapadnome dijelu tjesnaca Savu Strait od zadnjega ledenog maksimuma (~23 tis. god. pr. Kr.)

Unatoč svojoj važnosti paleoproduktivnost (morskoga stupca) zapadnoga dijela tjesnaca Savu nije dobro istražena. Rezultati prethodnih istraživanja na obližnjemu jugozapadnom dijelu Sumbe i u tjesnacu Sumba možda nisu primjenjivi zbog oceanografske razlike. Stoga su foraminifere prikupljene u jezgre ST10 uporabljene u ocjeni njihove paleoproduktivnosti te rekonstrukciji dubine termokline. Stopa akumulacije i iznos nakupljanja (bentičkih) foraminifera uporabljeni su za procjenu paleoproduktivnosti, dok je relativna brojnost organizama termokline korištena za procjenu njezine dubine. Rezultati upućuju na povećanje paleoproduktivnosti tijekom posljednjega ledenog doba (~16 tis. god. pr. Kr.) i holocena (mlađe od ~11,65 tis. god. pr. Kr.) u zapadnome dijelu tjesnaca Savu. Dubina termokline bila je manja tijekom zadnjega ledenog doba te početkom oledbe, a zatim je porasla. Povećanje paleoproduktivnosti kod posljednjega ledenog maksimuma prouzročeno je pojavom sličnom australsko-indonezijskomu zimskom monsunu, koji karakterizira intenzivno obalno uzdizanje. Nadalje, holocensko povećanje paleoproduktivnosti povezano je s naglim porastom oborina koje su povećale kopneni/riječni donos. Varijabilnost dubine termokline u zapadnome dijelu tjesnaca Savu tako je povezana s promjenama dubine termokline u prostoru Jave (koji se uzdiže), odnosno plića termoklina vezana je uz zadnji ledeni maksimum te prateću deglacijaciju (prije ~11,65 tis. god. pr. Kr.). Dublja termoklina opažena je u holocenu (nakon ~11,65 tis. god. pr. Kr.). Promjena dubine termokline upućuje na snažan utjecaj australsko-indonezijskoga monsunu na paleo-oceanografiju zapadnoga dijela tjesnaca Savu od zadnjega ledenog doba do danas.

Ključne riječi:

australsko-indonezijski monsun, stopa akumulacije foraminifera, indonezijski protok, paleoproduktivnost, Savu Strait

Author's contribution

Ryan Dwi Wahyu Ardi (1) (M. Sc., intern researcher, doctoral candidate, applied micropaleontologist, quaternary geologist) as the main contributor provided the micropaleontological analysis, paleoenvironmental interpretation, age-depth modeling, and presentation of the results. **Aswan (2)** (Dr., professor, quaternary geologist, paleontologist) provided paleoenvironmental interpretation and presentation of the results. **Khoiril Anwar Maryunani (3)** (Dr., assistant professor, applied micropaleontologist, paleoclimatologist, paleoceanographer) provided paleoenvironmental interpretation and paleoclimatological and paleoceanographic suggestions. **Eko Yulianto (4)** (Dr., researcher, quaternary geologist, palynologist) provided the paleoenvironmental interpretation and paleoclimatological ideas. **Purna Sulastya Putra (5)** (M. Sc., researcher, doctoral candidate, quaternary geologist, marine geologist) performed fieldwork and provided the regional marine geology and sedimentology views. **Septiriono Hari Nugroho (6)** (M. Sc., junior researcher, doctoral candidate, quaternary geologist, marine geologist) performed the fieldwork and provided the climate and oceanographic ideas.